Isobaric Heat Capacity of Solid and Liquid Thorium Tetrafluoride

Tosolin, Alberto; Capelli, Elisa; Konings, Rudy; Luzzi, Lelio; Beneš, Ondřej

DOI
10.1021/acs.jced.9b00348

Publication date
2019

Document Version
Final published version

Published in
Journal of Chemical and Engineering Data

Citation (APA)
Tosolin, A., Capelli, E., Konings, R., Luzzi, L., & Beneš, O. (2019). Isobaric Heat Capacity of Solid and Liquid Thorium Tetrafluoride. *Journal of Chemical and Engineering Data*, *64*(9), 3945-3950. https://doi.org/10.1021/acs.jced.9b00348

Journal of chemical & engineering data

Article

Cite This: J. Chem. Eng. Data 2019, 64, 3945−3950

pubs.acs.org/jced

Isobaric Heat Capacity of Solid and Liquid Thorium Tetrafluoride

Alberto Tosolin,*[,†,‡] Elisa Capelli,[§] Rudy Konings,[†,§] Lelio Luzzi,[‡] and Ondřej Beneš*[,†]

[†]European Commission, Joint Research Centre, P.O. Box 2340, 76125 Karlsruhe, Germany

[‡]Department of Energy, Politecnico di Milano, Via La Masa 34, 20156 Milan, Italy

[§]Department of Radiation Science & Technology, Delft University of Technology, Mekelweg 15, 2629 Delft, Netherlands

ABSTRACT: The isobaric heat capacity of solid and liquid thorium tetrafluoride was determined by two calorimetry methods: drop calorimetry to obtain the enthalpy increments in the range from 430 to 1600 K and DSC to obtain the high-temperature heat capacity of solid and liquid thorium tetrafluoride using the step method. Adjustments to the experimental setups were developed and implemented to increase accuracy and reduce uncertainty of the obtained data.

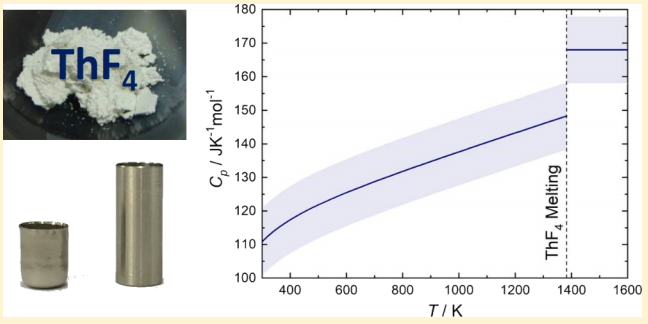

1. INTRODUCTION

In the last decades, the use of thorium in nuclear energy has been attracting great interest worldwide. Even though thorium-232 is not a fissile element, it can be transmuted into fissile uranium-233 by neutron absorption and two subsequent β-decay reactions: ${}^{232}_{90}\mathrm{Th} + \mathrm{n} \rightarrow {}^{233}_{90}\mathrm{Th} \rightarrow \beta^{-} {}^{233}_{91}\mathrm{Pa} \rightarrow \beta^{-} {}^{233}_{92}\mathrm{U}$.

Thorium is significantly more abundant in the Earth's crust than uranium, and the known ores (alluvial sands) require relatively easy mining operations. The identified resources are, however, significantly less. Thorium is available in significant quantities as byproducts of the rare-earth mining.

The use of thorium in nuclear reactors brings significant benefits:[1,2]

- Thorium fuels produce less minor actinides per energy generated compared to ^{235}U or ^{239}Pu-based fuel.
- For thermal neutrons, the absorption cross-section of ^{232}Th is almost three times higher than ^{238}U (^{232}Th is a better fertile material than ^{238}U).
- For ^{233}U, the number of neutrons emitted per neutron absorbed (represented as η) is greater than 2.0 for a very large energy range of the impacting neutron, unlike ^{235}U and ^{239}Pu for which breeding is basically possible only with fast neutrons.

In light of these advantages, the use of thorium has been considered in different reactor concepts, such as light-water reactors (LWRs),[3] heavy-water reactors (HWRs),[4] high-temperature gas-cooled reactors (HTGRs),[5] and molten salt reactors (MSRs).[6] In the latter one, fluoride salts are generally employed using ThF_4, the subject of this study, as one of the components.

In MSRs, the fuel is a mixture of molten salts (generally fluorides or chlorides) in which the nuclear fuel is dissolved.[7] As a result, there is no solid fuel element: in the core, there is a homogeneous liquid, allowing fuel cleanup either online or continuously.[8] The concept has other important benefits in terms of safety and sustainability.[9] For this reason, the Generation IV International Forum (GIF) selected the MSR as one of the six promising future reactors.[10] Several MSR concepts have been proposed and investigated, exploring different designs and applications.[11] Many of these concepts are proposed to utilize a closed Th/U fuel cycle and the deployment of fluoride mixtures as a fuel and coolant.

In this context, the isobaric heat capacity of solid and liquid ThF_4 fuel components is studied because reliable determination of the heat capacity as a function of temperature allows the investigation of many thermodynamic quantities such as enthalpy, entropy, Gibbs energy, and so on.[12,13] These thermodynamic functions are necessary for the calculation of phase diagrams[14] and the determination of properties at equilibrium[15] of systems containing ThF_4. Furthermore, the heat capacity is required (together with the density) to deduce thermal conductivity from thermal diffusivity.

The experimental investigation of high-temperature properties of ThF_4 still represents a challenge. Issues such as the high melting point and the volatility and corrosiveness of the halide vapor[16] (which can damage the instrument) must be taken into account. Furthermore, because ThF_4 is highly hygroscopic and may be sensitive to oxygen,[17] its manipulation and storage shall occur in gloveboxes under an inert atmosphere in which the content of oxygen and moisture is kept below a few parts per million. Because of these challenges, there is no experimental data in the literature for the high-temperature heat capacity of ThF_4.[18]

The issues described above were successfully faced in this work in which the heat capacity of solid and liquid thorium

Received: April 19, 2019
Accepted: August 8, 2019
Published: August 29, 2019

DOI: 10.1021/acs.jced.9b00348
J. Chem. Eng. Data 2019, 64, 3945−3950

Table 1. IUPAC Name, CAS Registry Number, Source, Purification Method and Final Sample Purity of the Chemicals Used in this Work

molecular formula	IUPAC name	CAS reg. no.	source	method	mass fraction purity
ThF_4	tetrafluorothorium	13709-59-6	synthesized	hydrofluorination	>99%
Ni	nickel	7440-02-0	Alfa Aesar		99.98%

tetrafluoride was revisited using well-established techniques, such as drop calorimetry and differential scanning calorimetry (DSC). To protect the devices from the corrosive fluoride vapors, samples were encapsulated using an in-house laser welding technique. A description of the experimental techniques and setups used in this work is given in Section 2. Results are presented in Section 3 and discussed in Section 4 together with the conclusions.

2. EXPERIMENTAL SECTION

2.1. Sample Preparation. Thorium tetrafluoride was synthesized by hydrofluorination of thorium dioxide using a HF line according to the reaction:

$$ThO_2 + 4HF \rightarrow ThF_4 + 2H_2O. \quad (1)$$

Purity of the obtained ThF_4 was checked by XRD and DSC (for melting point determination), indicating no impurities. For more details about the synthesis and the purity of the used ThF_4, we refer to our previous work.[19] Because fluorides are hygroscopic and sensitive to oxygen, ThF_4 was always handled in argon gloveboxes in which the content of oxygen and moisture is continuously monitored and kept below 2 ppm. Other info on the chemicals used in this work is given in Table 1.

For heat capacity measurements, ThF_4 was encapsulated in nickel (for chemical compatibility[20]) capsules, which consist of two parts (a container and a lid) sealed together by an in-house laser welding technique described in our previous work.[21] After insertion of ThF_4 into the container, the lid is pressed manually at the top and then welded with a laser. The quality of the welding is first checked visually by microscopy and then tested by heating up to 1523 K for 4 h in an argon atmosphere, monitoring any weight loss. The experience shows that in case of a leak, the weight of the sample after the heating process will be lower because some material escapes in the form of vapor.

Three samples were prepared for drop calorimetry. For measurement by DSC, a crucible with a total height of 12 mm was made, increasing the ratio between the mass of ThF_4 and the one of the capsule. The characteristics of the samples used for measurements by drop and DSC are summarized in Table 2.

2.2. Drop Calorimetry. Enthalpy increments were measured using a Setaram multidetector high-temperature calorimeter (MHTC 96) equipped with a drop sensor with B-type thermocouples, allowing measurements from room temperature to 1773 K. Calibration of the device was performed using a series of reference materials. Type B uncertainty on temperature is ±1 K.

The experimental chamber was flushed with argon to prevent oxidation of the nickel capsule. The samples, initially at room temperature (298 K), were dropped into the furnace stabilized at a fixed temperature. Immediately after the drop, additional heat is provided by the furnace to restore the initial temperature. This additional heat is monitored by a series of thermocouples and is proportional to the enthalpy increment of the dropped sample from room temperature to the temperature of the furnace. The device is equipped with an automatic multisample introducer, which allows consecutive drops of several samples. Each experiment consisted of seven drops: three encapsulated ThF_4 samples (listed in Table 2) and four pieces of the nickel reference material for calibration. Each drop is separated by 25 min intervals, enough to re-establish a constant heat flow signal. Since ThF_4 is encapsulated in a crucible, the contribution of the capsule (which is made of nickel, the properties of which are well known) must be subtracted so that the formula for the enthalpy increment of ThF_4 is

$$\Delta H_{ThF_4} = \frac{A_{sam}}{A_{ref}} \Delta H_{ref} - \Delta H_{cruc} \quad (2)$$

where A_{sam} and A_{ref} are the values of the areas under the peaks (in $\mu V \cdot s$) provided by the drop of the sample (ThF_4 + capsule) and the reference, respectively. ΔH_{ref} and ΔH_{cruc} are the enthalpy increments of the reference and of the nickel capsule, respectively. Their values were determined according to the masses employed in the experiments and specific enthalpy values reported in the literature.[22,23] Tests performed with characterized materials for both samples and references pointed out a systematic deviation from the expected results if A_{sam} and A_{ref} differ significantly. This loss of accuracy increases with temperature and led to uncertain results in previous attempts to measure the high-temperature heat capacity of ThF_4 by drop calorimetry.[24] Because of this, the references used in this work were selected to have $A_{ref} \approx A_{sam}$.

After several experiments performed at different temperatures T and normalizing enthalpy values per mole, a regression function can be applied to the $(H^T - H^{298})$ versus T diagram, whose derivative gives the isobaric heat capacity:

$$C_p = \frac{dH}{dT} \quad (3)$$

2.3. Differential Scanning Calorimetry. The high-temperature heat capacity of solid and liquid ThF_4 was measured by DSC using a Setaram multidetector high-temperature calorimeter (MHTC 96), installed in an argon glovebox and equipped with a DSC sensor with a B-type thermocouple, allowing measurements from room temperature to 1873 K (a bit higher than drop calorimetry, in agreement with the recommendations provided by Setaram when the device operates in DSC mode). Calibration of the device was performed using a series of reference materials. Long-time experience indicates that the time constant of the instrument can be accounted for by assuming that the response of metallic

Table 2. Mass m and Height h of the Samples Used in This Work[a]

sample	capsule h (mm)	m(tot) (mg)	m(Ni) (mg)	m(ThF_4) (mg)	technique
sample 1	6.0	363.5	251.2	112.3	drop
sample 2	6.0	348.1	236.9	111.2	drop
sample 3	6.0	350.9	242.4	108.5	drop
sample 4	12.0	992.1	580.2	411.9	DSC

[a]Standard uncertainty of mass $u(m)$ is 0.5 mg.

DOI: 10.1021/acs.jced.9b00348
J. Chem. Eng. Data 2019, 64, 3945−3950

references is similar to the salt itself. Type B uncertainty on temperature is ±1 K.

The experimental chamber is divided into two compartments in which nickel liners are inserted to protect the detector in case of crucible failure during the experiments. Liners have an inner diameter of 6.5 mm and a working height of 16 mm. Acquisition and post-processing of the data were carried out using AKTS Calisto software v1.10.[25]

The experiments were conducted according to the "classical" three step procedure,[26] with some adjustments suitable for taking into account the presence of the capsule. Once a temperature step program was set, three experiments were performed to collect all data needed for the heat capacity determination. The three experiments consisted of the same temperature step program but with different experimental setups, as described below.

A sealed empty capsule was inserted into the DSC reference compartment and left there during the entire experimental campaign, which consisted of groups of three experiments, loading in the sample compartment in succession:

1. an empty capsule (blank run);
2. a capsule filled with ThF_4 (sample run); and
3. a capsule filled with a piece of nickel reference material (reference run).

Considering a single temperature step, the three experiments gave clear peaks on the heat flow curve. The peaks were first smoothed using a Gaussian function, and their underlying area was calculated using a tangential sigmoid function as the integration baseline. The obtained values were named A_{bla}, A_{sam}, and A_{ref} to identify the values obtained by the experiment with the empty capsule (blank), the ThF_4 sample (sample), and the reference material (reference), respectively. The molar isobaric heat capacity of ThF_4 was then determined using the following formula:

$$C_p(ThF_4) = \frac{n_{ref}}{n_{sam}} C_p(ref) \frac{A_{sam} - A_{bla}}{A_{ref} - A_{bla}} \quad (4)$$

where $C_p(ref)$ is the heat capacity of the reference material and n_{ref} and n_{sam} are the number of moles of the reference material and the ThF_4 sample, respectively.

It is important to notice that eq 4 is reliable only if all capsules put in the DSC compartments (before the filling) have the same mass. Capsules used in this work were selected following this guideline, with the weight discrepancy less than ±0.5 mg. Furthermore, the nickel reference was selected to have $A_{ref} \approx A_{sam}$.

Due to repeatability problems, different experimental setups were tested to identify the source of error, as discussed in Section 3.2. The results presented in this paper were performed using temperature steps of 100 K, a heating rate of 10 K/min, and 2 h for signal stabilization prior to each step, as shown in Figure 1.

3. RESULTS

3.1. Drop Calorimetry. Measurements were performed from 430 to 1601 K with steps of ~50 K up to 686 K and of 100 K above. For the liquid phase, measurements at 1499 and 1601 K were performed. Results are summarized in Table 3.

The enthalpy increments reported are the average values of different measurements performed at the given temperature. We note that the standard uncertainties are higher than typical values obtained by drop calorimetry. This is due to the high volume and mass of the samples dropped and to the contribution of nickel used for encapsulation, which must be subtracted. In this regard, as explained in Section 2.1, the mass of the nickel capsule is considerably higher than the mass of the thorium tetrafluoride inside (see Table 2), and this affects the uncertainty.

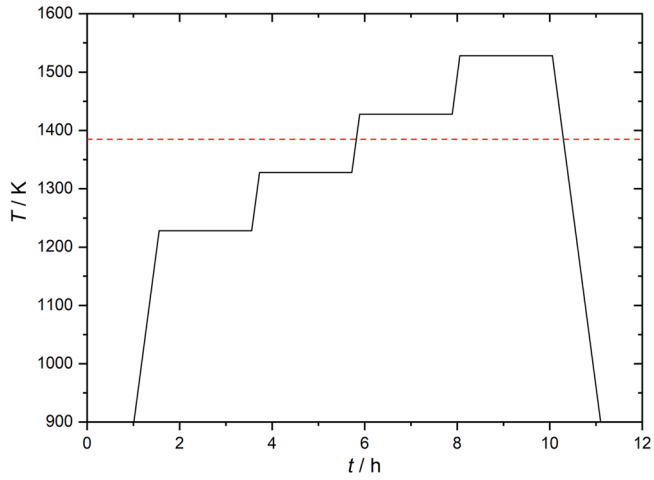

Figure 1. DSC temperature program used in this work for heat capacity determination (solid black line) and ThF_4 melting point (red dashed line).

Table 3. Molar Enthalpy Increments ($H^T - H^{298}$) of Solid and Liquid ThF_4 and Related Standard Uncertainty *St. u* as a Function of Temperature *T*[a]

T (*K*)	$(H^T - H^{298})$ (kJ·mol^{-1})	*St. u* (kJ·mol^{-1})	*n* drops
430	17.1	2.6	3
483	27.0	4.1	6
534	33.5	6.0	6
585	37.3	5.6	2
637	47.3	7.1	5
686	51.7	8.5	6
788	62.8	13.2	6
889	73.4	11.9	3
991	95.4	12.3	5
1091	107.5	14.9	5
1193	114.7	8.2	6
1295	131.6	11.7	5
1499 (liq)	199.9	8.5	5
1601 (liq)	216.6	17.3	5

[a]Last column reports the number of drops. Measurements were performed at atmospheric pressure. Uncertainty on temperature values is 1 K.

Derivatives of the linear fits (obtained using the least-squares approach and imposing the zero value at 298.15 K for the solid phase) give an average heat capacity of 133.4 ± 3.5 J·K^{-1}·mol^{-1} from room temperature to the melting point and a value of 162 ± 69 J·K^{-1}·mol^{-1} for the liquid phase. Given uncertainties are standard deviations in the slope of the linear fits based on the enthalpy increment data summarized in Table 3. We note that the value for the solid phase is the mean value considering a large temperature range. Measurements in the liquid state were performed in a short temperature range due to the high melting point T_m of ThF_4 (1383 ± 3 K)[18] and the instrumental limit of our device (Section 2.2).

The enthalpy of fusion obtained by extrapolating the linear fits for the solid and the liquid phase up to 1383 K is 36.4 kJ·mol^{-1}, and an indicative estimated uncertainty of 10 kJ·mol^{-1} is applied

DOI: 10.1021/acs.jced.9b00348
J. Chem. Eng. Data 2019, 64, 3945−3950

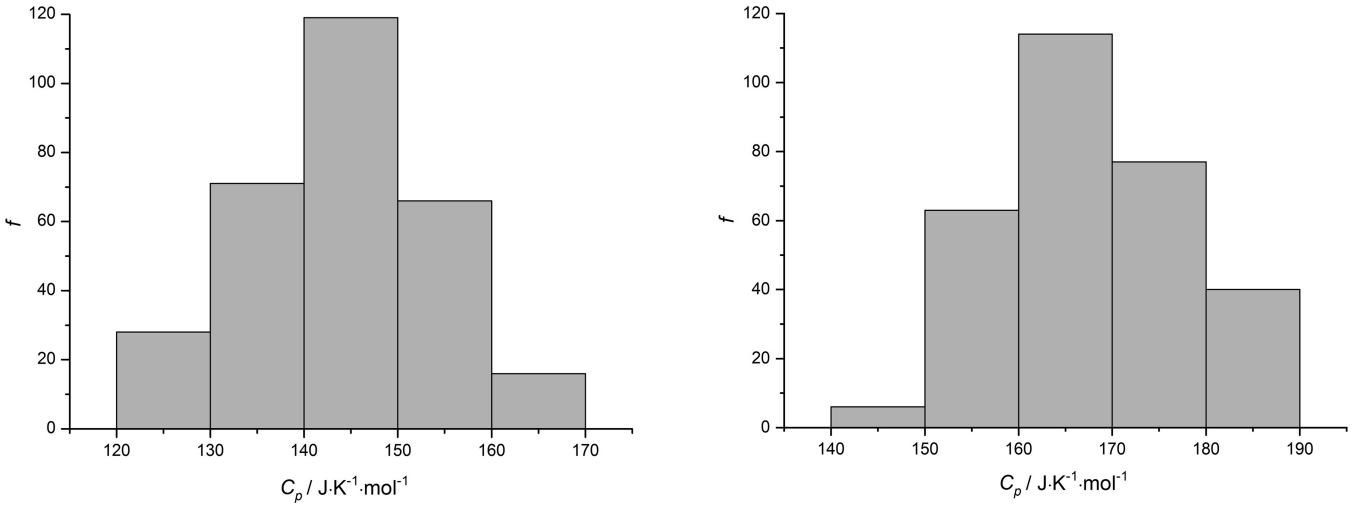

Figure 2. Histograms obtained with 300 extractions or random values between A_i^{min} and A_i^{max}(i = sam, bla, ref). Results on the left refer to the temperature step from 1228 and 1328 K (solid ThF_4). Results on the right refer to a temperature step program from 1428 and 1528 K (liquid ThF_4).

considering the error bars of the enthalpy increment data in the liquid phase. This is in reasonable agreement with the value measured in our previous work,[27] determined to be 41.9 kJ·mol^{-1}. This value was measured by the DSC technique, and an uncertainty of ±2.0 kJ·mol^{-1} was reported.

3.2. Differential Scanning Calorimetry. Each experiment was repeated three times (3 times for the blank, 3 times for the ThF_4 sample, and 3 times for the reference), and the values of the areas under the peaks were collected. Because there was no evidence to assume that some measurements were more reliable than others, we extracted 300 random values (assuming a uniform probability distribution) between the minimum and the maximum values of the heat flow areas for each temperature step, and we combined these values randomly for calculating heat capacity values according to eq 4, collecting values within the range 120 to 170 J·K^{-1}·mol^{-1} for the solid phase and within 140 to 190 J·K^{-1}·mol^{-1} for the liquid phase. Following this approach, histograms in Figure 2 were obtained. The figure on the left refers to the temperature step from 1228 and 1328 (solid ThF_4). The one on the right refers to the temperature step from 1428 to 1528 (liquid ThF_4).

We notice that using temperature steps of 100 K, we lose information on the heat capacity behavior within the considered step. This was necessary to overcome the large uncertainty, which affected heat capacity values using smaller steps. Lids for the liners of the DSC compartments were re-designed to achieve better positioning and closure, which was found to be an important factor improving experimental repeatability.

The obtained heat capacity results are listed in Table 4 in which given uncertainties are the standard deviations of the values shown in Figure 2.

Table 4. Heat Capacity (C_p) Results of Solid and Liquid ThF_4, Related Standard Uncertainties *St. u*, and Average Values of the Temperature Steps Used in the DSC Program (T_{av})[a]

compound	T_{av} (K)	C_p (J·K^{-1}·mol^{-1})	*St. u* (J·K^{-1}·mol^{-1})
ThF_4 (sol)	1278	145	10
ThF_4 (liq)	1478	168	10

[a]Measurements were performed at atmospheric pressure.

We note that the values obtained by DSC are in good agreement with results obtained by drop calorimetry.

4. DISCUSSION AND CONCLUSIONS

In this section, the results presented in Section 3 are discussed and used to determine the heat capacity for a wide range of temperatures. Available literature data are used for comparison.

To determine the high-temperature heat capacity of solid ThF_4, a simultaneous linear regression was used with the following constraints and guidelines:

- The heat capacity at 298.15 K should fit the value measured by Lohr et al.[28] (110.7 J·K^{-1}·mol^{-1}) who performed measurements from 5.54 to 298.17 K. A smooth transition between low- and high-temperature heat capacity was maintained.
- The heat capacity at 1278 K should fit the value of 145 J·K^{-1}·mol^{-1} measured in this work (Section 3.2) by DSC.
- Experimental uncertainties were considered during the fitting procedure.

Based on this approach, we propose an equation for the heat capacity of solid and liquid ThF_4 of the form:

$$C_p\ (\mathrm{J{\cdot}K^{-1}{\cdot}mol^{-1}}) = a + b\,T + c\,T^{-2} \quad (5)$$

where *a*, *b*, and *c* are defined in Table 5. For both phases, the heat capacity is affected by an uncertainty of ±10 J·K^{-1}·mol^{-1}, in agreement with values in Table 4. Temperature ranges of applicability for coefficients in Table 5 are 298 to T_m for the solid phase and T_m to 1600 K for the liquid phase.

Table 5. Coefficients for C_p (J·K^{-1}·mol^{-1}) of Solid and Liquid ThF_4[a]

	C_p (J·K^{-1}·mol^{-1}) = $a + b\,T + c\,T^{-2}$		
compound	*a*	*b*	*c*
ThF_4 (sol)	111.46	2.69×10^{-2}	-7.80×10^{5}
ThF_4 (liq)	168	0	0

[a]For both phases, the heat capacity is affected by an uncertainty of ±10 (J·K^{-1}·mol^{-1}). Temperature ranges of applicability are 298 K to T_m for the solid phase and T_m to 1600 K for the liquid phase.

DOI: 10.1021/acs.jced.9b00348
J. Chem. Eng. Data 2019, 64, 3945−3950

For the solid phase, values obtained using eq 5 are shown in Figure 3 as a solid black line.

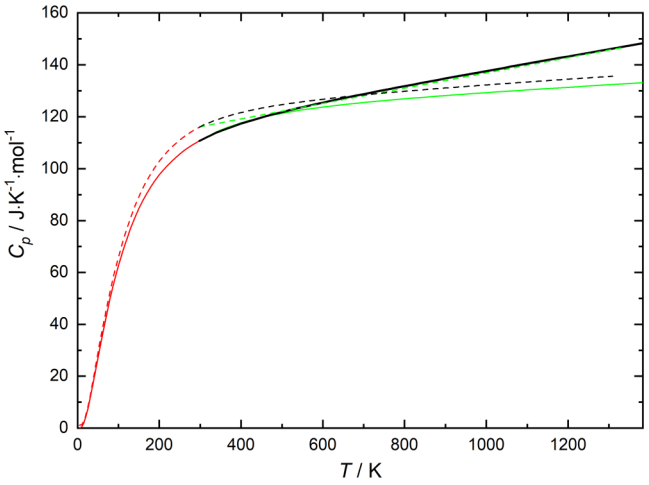

Figure 3. Isobaric heat capacity values of solid ThF_4 obtained in this work (solid black line) and comparison with ThF_4 heat capacity data by Lohr et al.[28] (solid red line) and Wagman et al.[29] (solid green line), and UF_4 heat capacity data by Osborne et al.[30] (dashed red line), King and Christensen[31] (dashed green line), and Dworkin[32] (dashed black line).

Low-temperature (LT) heat capacity values measured by Lohr et al.[28] are also shown in Figure 3 (solid red line). To the best of our knowledge, no other measurements were published for the heat capacity of solid ThF_4. The solid green line shows the heat capacity values suggested by Wagman et al.[29] based on enthalpy measurements by Dworkin, who declared experimental difficulties and did not complete the measurements.[32] As shown in Figure 3, our data give results that are a bit higher than the ones suggested by Wagman with maximum deviation upon the melting point of approximately 14 J·K^{-1}·mol^{-1}.

Because of the lack of experimental data, we also compare our data with available measurements for UF_4, which has chemical[33] and structural[19] similarities with ThF_4. Results for UF_4 are represented as dashed lines. Several authors[30,34,35] performed measurements at low temperature. Results are all in excellent agreement, so we represent (for the sake of clarity) only the values by Osborne et al.[30] High-temperature (HT) values obtained by King and Christensen[31] (green dashed line) and Dworkin[32] (black dashed line) are also shown in Figure 3. Values suggested by King and Christensen[31] for UF_4 are very close to the ones suggested in this work for ThF_4. The formula suggested by Dworkin for UF_4 gives a similar trend to the one suggested by Wagman for ThF_4, with a rather constant shift of ~4 J·K^{-1}·mol^{-1}.

As shown in Table 5, for the heat capacity of liquid ThF_4, we suggest a constant value, with respect to a general trend for many fluorides.[18,36] The selected value of 168 ± 10 J·K^{-1}·mol^{-1} obtained by DSC in the step method is in good agreement with the result obtained using drop calorimetry (Section 3.1). Wagman et al.[29] proposed an approximate value for liquid ThF_4 equal to 134 J·K^{-1}·mol^{-1}. This value, which is also based on results by Dworkin, is 20% lower than that in our measurement. In this regard, we note that we made similar conclusions also for the solid phase. Since there is no other data in the literature for the heat capacity of liquid ThF_4, we compare our result with the value calculated using the approximated formula suggested by Khokhlov et al.:[37]

$$c_p\ (J{\cdot}K^{-1}{\cdot}g^{-1}) = (0.2916 \pm 0.0404) + (0.00802 \pm 0.216 \times 10^{-3}) \times 10^4/M \quad (6)$$

As explained in their paper, the formula is based on the empirical observation that the heat capacity (if expressed in J·K^{-1}·g^{-1}) of molten fluorides and their mixtures has a rather linear dependence on the reciprocal molar mass (1/M). The uncertainty band obtained from eq 6 includes many experimental values and does not exceed the typical uncertainty of measuring the heat capacity of salt melts indicated by most research studies (3 to 10%).[38] For ThF_4, eq 6 gives a value of 170 ± 15 J·K^{-1}·mol^{-1}, which is in very good agreement with our experimental result.

In view of the mentioned similarities between ThF_4 and UF_4, we compare our result for the liquid with the heat capacity of liquid UF_4 measured by Dworkin[32] and King and Christensen,[31] who suggested 166 and 167 J·K^{-1}·mol^{-1}, respectively. Both values were derived by enthalpy data and are in very good agreement with each other (despite the different conclusions these authors made for the solid phase) and with our result for ThF_4. The value of 170 J·K^{-1}·mol^{-1} estimated by Capelli et al.[27] from phase diagram optimization is also in excellent agreement with our experimental results.

Finally, the enthalpy increment values obtained by integration of the heat capacity for both solid and liquid ThF_4 (solid red line) are shown in Figure 4 together with the drop calorimetry data obtained in this work (black markers with error bars).

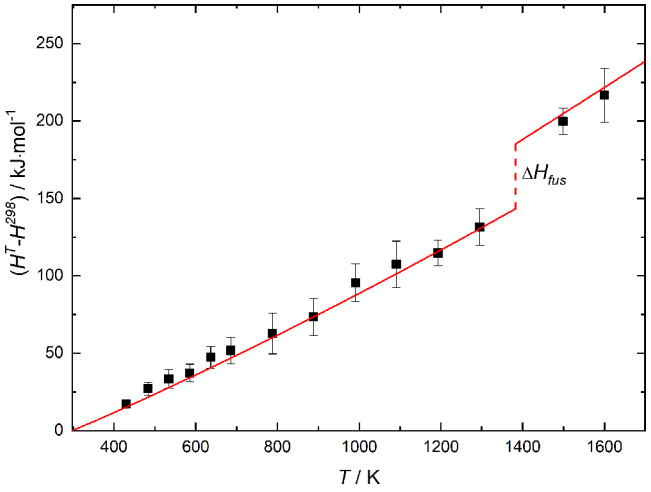

Figure 4. Enthalpy increment values obtained integrating the heat capacity of solid and liquid ThF_4 proposed in this work (solid red line). Results obtained in this work by drop calorimetry (black markers, ■) are also shown for comparison.

The solid red line was determined imposing the zero value at 298.15 K and using the enthalpy of fusion measured in our previous work (41.9 ± 2.0 kJ·mol^{-1}) as boundary conditions for the solid and liquid phases, respectively. The agreement between our drop calorimetry results and the integral of the heat capacity is quite good.

AUTHOR INFORMATION

Corresponding Authors

*E-mail: alberto.tosolin@polimi.it (A.T.).
*E-mail: Ondrej.BENES@ec.europa.eu (O.B.).

ORCID

Alberto Tosolin: 0000-0001-9918-7933

DOI: 10.1021/acs.jced.9b00348
J. Chem. Eng. Data 2019, 64, 3945−3950

Elisa Capelli: 0000-0002-8988-4310

Notes

The authors declare no competing financial interest.

■ ACKNOWLEDGMENTS

This work has been funded by the Euratom research and training programme 2014-2018 under grant agreement no. 661891 (SAMOFAR). A.T. acknowledges the Joint Research Centre (JRC) for providing access to its research infrastructure. This work has been partially supported by the ENEN+ project that has received funding from the Euratom research and training Work Programme 2016 − 2017 − no. 755576. A.T. would like to thank his current employer, Canadian Nuclear Laboratories (CNL), for the courtesy extended, allowing him to finish this article.

■ REFERENCES

(1) International Atomic Energy Agency *Thorium Fuel Cycle—Potential Benefits and Challenges*; International Atomic Energy Agency: 2005.

(2) Nuclear Energy Agency. *Introduction of Thorium in the Nuclear Fuel Cycle*; Organisation for Economic Co-operation and Development: 2015.

(3) Todosow, M.; Galperin, A.; Herring, S.; Kazimi, M.; Downar, T.; Morozov, A. Use of Thorium in Light Water Reactors. *Nucl. Technol.* **2005**, *151*, 168−176.

(4) Sinha, R. K.; Kakodkar, A. Design and Development of the AHWR-the Indian Thorium Fuelled Innovative Nuclear Reactor. *Nucl. Eng. Des.* **2006**, *236*, 683−700.

(5) Shamanin, I.; Bedenko, S.; Chertkov, Y.; Gubaydulin, I. Gas-Cooled Thorium Reactor with Fuel Block of the Unified Design. *Adv. Mater. Sci. Eng.* **2015**, *2015*, 184−190.

(6) Heuer, D.; Merle-Lucotte, E.; Allibert, M.; Brovchenko, M.; Ghetta, V.; Rubiolo, P. Towards the Thorium Fuel Cycle with Molten Salt Fast Reactors. *Ann. Nucl. Energy* **2014**, *64*, 421−429.

(7) Dolan, T. J., Ed.; *Molten Salt Reactors and Thorium Energy*; Woodhead Publishing: 2017, Cambridge.

(8) Delpech, S.; Merle-Lucotte, E.; Heuer, D.; Allibert, M.; Ghetta, V.; Le-Brun, C.; Doligez, X.; Picard, G. Reactor Physic and Reprocessing Scheme for Innovative Molten Salt Reactor System. *J. Fluorine Chem.* **2009**, *130*, 11−17.

(9) Luzzi, L.; Aufiero, M.; Cammi, A.; Fiorina, C. Thermo-Hydrodynamics of Internally Heated Molten Salts for Innovative Nuclear Reactors. In *Hydrodynamics - Theory and Model*; Zheng, J., Ed.; InTech: 2012, pp 119−142.

(10) Nuclear Energy Agency *Technology Roadmap Update for Generation IV Nuclear Energy Systems*; Organisation for Economic Co-operation and Development: 2014.

(11) Serp, J.; Allibert, M.; Beneš, O.; Delpech, S.; Feynberg, O.; Ghetta, V.; Heuer, D.; Holcomb, D.; Ignatiev, V.; Kloosterman, J. L.; et al. The Molten Salt Reactor (MSR) in Generation IV: Overview and Perspectives. *Prog. Nucl. Energy* **2014**, *77*, 308−319.

(12) Beneš, O.; Konings, R. J. M. Actinide Burner Fuel: Potential Compositions Based on the Thermodynamic Evaluation of MF-PuF_3 (M = Li, Na, K, Rb, Cs) and LaF_3-PuF_3 Systems. *J. Nucl. Mater.* **2008**, *377*, 449−457.

(13) Capelli, E.; Beneš, O.; Konings, R. J. M. Thermodynamic Assessment of the LiF-ThF_4-PuF_3-UF_4 system. *J. Nucl. Mater.* **2015**, *462*, 43−53.

(14) Tosolin, A.; Souček, P.; Beneš, O.; Vigier, J.-F.; Luzzi, L.; Konings, R. J. M. Synthesis of Plutonium Trifluoride by Hydro-Fluorination and Novel Thermodynamic Data of PuF_3 -LiF System. *J. Nucl. Mater.* **2018**, *503*, 171−177.

(15) Tosolin, A.; Beneš, O.; Colle, J.-Y.; Souček, P.; Luzzi, L.; Konings, R. J. M. Vaporization Behaviour of the Molten Salt Fast Reactor Fuel: The LiF-ThF_4 -UF_4 System. *J. Nucl. Mater.* **2018**, *508*, 319−328.

(16) Davidovits, P., McFadden, D. L., Eds.; *Alkali Halide Vapors: Structure, Spectra, and Reaction Dynamic*; Academic Press, Inc.: 1979, Cambridge, Massachusetts.

(17) Mukherjee, S.; Dash, S.; Mukerjee, S. K.; Ramakumar, K. L. Thermodynamic Investigations of Oxyfluoride of Thorium and Uranium. *J. Nucl. Mater.* **2015**, *465*, 604−614.

(18) Nuclear Energy Agency *Chemical Thermodynamics of Thorium*; Organisation for Economic Co-operation and Development; 2007.

(19) Souček, P.; Beneš, O.; Claux, B.; Capelli, E.; Ougier, M.; Tyrpekl, V.; Vigier, J.-F.; Konings, R. J. M. Synthesis of UF_4 and ThF_4 by HF Gas Fluorination and Re-Determination of the UF_4 Melting Point. *J. Fluorine Chem.* **2017**, *200*, 33−40.

(20) Briggs, R. B. *Molten-Salt Reactor Program Semiannual Progress Report for Period Ending July 31, 1964*. ORNL-*3708*; 1964.

(21) Beneš, O.; Konings, R. J. M.; Kuenzel, C.; Sierig, M.; Dockendorf, A.; Vlahovic, L. The High-Temperature Heat Capacity of the (Li, Na)F Liquid Solution. *J. Chem. Thermodyn.* **2009**, *41*, 899−903.

(22) Ditmars, D. A.; Ishihara, S.; Chang, S. S.; Bernstein, G.; West, E. D. Enthalpy and Heat-Capacity Standard Reference Material: Synthetic Sapphire (Alpha-Al_2O_3) From 10 to 2250 K. *J. Res. Natl. Bur. Stand.* **1982**, *87*, 159.

(23) Desai, P. D. Thermodynamic Properties of Nickel. *Int. J. Thermophys.* **1987**, *8*, 763−780.

(24) Capelli, E. *Thermodynamic Characterization of Salt Components for Molten Salt Reactor Fuel*, Delft University of Technology: 2015.

(25) AKTS. Calisto processing software http://www.akts.com/tga-dsc-dta-tma-ftir-ms-analysis-software/download-calisto-processing-software.html (accessed May 15, 2018).

(26) Höhne, G. W. H.; Hemminger, W.; Flammersheim, H.-J. *Differential Scanning Calorimetry*; Springer: Berlin Heidelberg, 1996.

(27) Capelli, E.; Beneš, O.; Beilmann, M.; Konings, R. J. M. Thermodynamic Investigation of the LiF-ThF_4 System. *J. Chem. Thermodyn.* **2013**, *58*, 110−116.

(28) Lohr, H. R.; Osborne, D. W.; Westrum, E. F., Jr. Thermodynamic Properties of Thorium Tetrafluoride from 5 to 300°K. and the Magnetic Entropy of Uranium Tetrafluoride. *J. Am. Chem. Soc.* **1954**, *76*, 3837−3839.

(29) Wagman, D. D.; Schumm, R. H.; Parker, V. B. *Computer-Assisted Evaluation of the Thermochemical Data of the Compounds of Thorium*; National Bureau of Standards: 1977, No. NBSIR 77−1300.

(30) Osborne, D. W.; Westrum, E. F., Jr.; Lohr, H. R. The Heat Capacity of Uranium Tetrafluoride from 5 to 300 °K. *J. Am. Chem. Soc.* **1955**, *77*, 2737−2739.

(31) King, E. G.; Christensen, A. U. *High-Temperature Heat Content of Uranium Tetrafluoride*; US Bereau of Mines, Technical Report BMI Report 5709, 1961.

(32) Dworkin, A. S. Enthalpy of Uranium Tetrafluoride from 298−1400°K: Enthalpy and Entropy of Fusion. *J. Inorg. Nucl. Chem.* **1972**, *34*, 135−138.

(33) Beneš, O.; Beilmann, M.; Konings, R. J. M. Thermodynamic Assessment of the LiF−NaF−ThF_4−UF_4 system. *J. Nucl. Mater.* **2010**, *405*, 186−198.

(34) Brickwedde, F. G.; Hoge, H. J.; Scott, R. B. The Low Temperature Heat Capacities, Enthalpies, and Entropies of UF_4 and UF_6. *J. Chem. Phys.* **1948**, *16*, 429−436.

(35) Burns, J. H.; Osborne, D. W.; Westrum, E. F., Jr. Heat Capacity of Uranium Tetrafluoride from 1.3° to 20°K and the Thermodynamic Functions to 300°K. Calorimeter for the Range 0.8° to 20°K. *J. Chem. Phys.* **1960**, *33*, 387−394.

(36) Powers, W. D.; Cohen, S. I.; Greene, N. D. Physical Properties of Molten Reactor Fuels and Coolants. *Nucl. Sci. Eng.* **1963**, *17*, 200−211.

(37) Khokhlov, V.; Ignatiev, V.; Afonichkin, V. Evaluating Physical Properties of Molten Salt Reactor Fluoride Mixtures. *J. Fluorine Chem.* **2009**, *130*, 30−37.

(38) Kelley, K. K. Contributions to the Data on Theoretical Metallurgy. *US Bur. Mines Bull.*; United States Government Printing Office: Washington, 1960, *584*.

DOI: 10.1021/acs.jced.9b00348
J. Chem. Eng. Data 2019, 64, 3945−3950